IOPscience iopscience.iop.org

Home Search Collections Journals About Contact us My IOPscience

High pressure and temperature behaviour of electrical resistivity of hcp metals Ti, Zr and Gd

This article has been downloaded from IOPscience. Please scroll down to see the full text article.

1999 J. Phys.: Condens. Matter 11 1273

(http://iopscience.iop.org/0953-8984/11/5/014)

View the table of contents for this issue, or go to the journal homepage for more

Download details:
IP Address: 171.66.16.214
The article was downloaded on 15/05/2010 at 06:57

Please note that terms and conditions apply.

J. Phys.: Condens. Matter **11** (1999) 1273–1287. Printed in the UK PII: S0953-8984(99)95944-1

High pressure and temperature behaviour of electrical resistivity of hcp metals Ti, Zr and Gd

Paul S Balog and Richard A Secco†

Department of Earth Sciences, University of Western Ontario, London, Ontario N6A 5B7, Canada

Received 14 July 1998, in final form 9 November 1998

Abstract. High pressure measurements of electrical resistivity of polycrystalline Ti, Zr and Gd have been performed in the temperature range 22–1000 °C and in the pressure range 4–48 kbar. The pressure and temperature coefficients of electrical resistivity of the hcp phase have been determined and new measurements of the boundaries into hcp-neighbouring phases are presented. All three metals show typical pressure and temperature dependences of resistivity behaviour in the hcp region, with Gd displaying the greatest sensitivity to pressure due to its high compressibility.

1. Introduction

At room temperature and pressure Ti, Zr and Gd are hexagonal close-packed (hcp) metals with incompletely filled d bands and a c/a axial ratio of 1.59, while at high temperatures they adopt a body-centred-cubic (bcc) structure. The phase diagrams of the three elements are shown in figure 1 [1, 2]. One of the first sets of high pressure phase diagrams and transport measurements on Ti and Zr was performed by Bridgman [3, 4] and his data stand as a reference. Many later studies have reported data on the pressure–temperature (P–T) phase diagram and the crystal structure of Ti and Zr [5–13], mainly using *in situ* X-ray diffraction and electrical resistivity techniques.

At room temperature, the hcp phases of Ti and Zr are stable up to 20–25 kbar, where they undergo a transformation into dhcp phase (β-Po type). The high pressure dhcp phase persists after pressure release, and the recovery of the hcp phase requires heating to 300 °C. At 1 atm, Ti and Zr undergo another transformation into the bcc phase at temperatures just above 850 °C, before melting at approximately 1200 °C. For the high pressure hcp → dhcp (β-Po type) transformation at room temperature in Ti and Zr, the results attest to the presence of both phases in an interval from 15 to 55 kbar. The phase equilibrium boundary is presently represented in the phase diagrams of Ti and Zr as an intermediate slope between the region of complete dhcp phase and complete hcp phase. At temperatures above 300 °C, the hysteresis is effectively zero. An alternative explanation for the large differences in transition pressures reported in the various studies was given by Olinger and Jamieson [8] and Andersson [14], who suggested that the hcp → dhcp transformation is aided by the presence of oxygen, especially in the case of powdered samples of Ti or Zr. In the same context, it has been shown by numerous groups [3–6, 11, 12] that the rate of the hcp → dhcp transformation depends on the purity of the material, the degree of hydrostaticity and the specimen history.

† Corresponding author. E-mail address: secco@julian.uwo.ca.

0953-8984/99/051273+15$19.50 © 1999 IOP Publishing Ltd

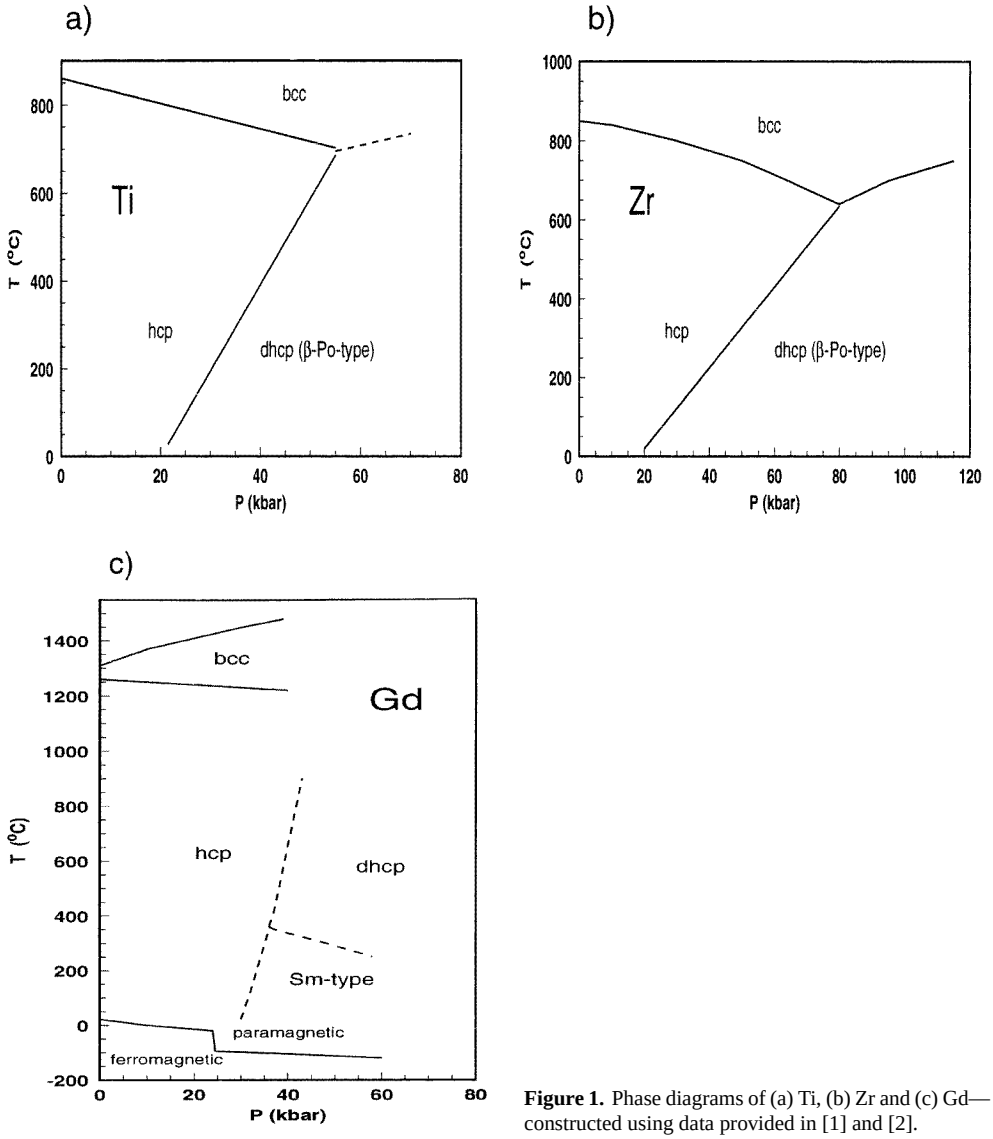

Figure 1. Phase diagrams of (a) Ti, (b) Zr and (c) Gd—constructed using data provided in [1] and [2].

Measurements of electrical resistivity of polycrystalline Ti and Zr have been performed mostly at low and atmospheric pressure [15–21]. Wasilewski [18] and Zinov'yev [20] have measured the electrical resistivity of single crystal Ti in the hcp phase region and showed the existence of anisotropy of resistivity. The number of studies reporting electrical resistivity measurements of Ti and Zr at elevated pressure is limited [6, 13, 22, 23], but these experiments have made significant contributions to the mapping of the P–T phase diagrams of Ti and Zr.

At high pressure, Gd transforms from hcp into a hexagonal structured Sm-type phase, but the phase boundary is not well determined. Different experimental methods have shown the beginning of the Sm-type phase in an interval from 15 to 30 kbar [24–27]. At 1 atm and elevated temperature, a transformation into bcc occurs at 1250 °C and the melting is recorded at about 1350 °C.

The high pressure resistivity and compressibility of Gd was reported by Bridgman [24]. Bridgman detected a change in R/R_0 with pressure increase, between 20 and 25 kbar, and considered it an anomaly. On pressure decrease, the reversal does not occur. Later experiments [27–29] have confirmed the presence of a large hysteresis in the Sm type $\rightarrow$ hcp transformation.

The 1 atm high temperature electrical resistivity of Gd was measured by Spedding *et al* [30] up to 1350 °C and was used to determine the hcp $\rightarrow$ bcc transformation. The effect of temperature on the electrical resistivity of polycrystalline Gd was reported in a number of other studies [31–33]. Measurements of the electrical and thermal transport properties of single crystal Gd at 1 atm have revealed the presence of anisotropy of electrical resistivity in the hcp range [34–39]. The combined effect of high pressure and high temperature on the electrical properties of Gd above the Curie temperature has been reported in only one study [40].

Most of the high pressure studies of Gd have concentrated on the determination of the phase diagram and on the effect of pressure on the Curie temperature [6, 23, 25, 41–43]. Using a four wire technique, Stromberg and Stephens [44] measured the pressure dependence of electrical resistivity of Gd up to 140 kbar, but the sampling interval was too large to allow for the accurate mapping of the hcp $\rightarrow$ Sm type phase boundary. At pressures higher than 35 kbar and at temperatures above 300 °C, Gd undergoes another structural transformation from Sm type to dhcp [25, 28]. The hcp $\rightarrow$ dhcp $\rightarrow$ Sm type triple point is at about 37 kbar and 340 °C. However, not all phase diagrams agree with these values and the phase boundaries between hcp $\rightarrow$ Sm type and hcp $\rightarrow$ dhcp are still the subject of controversy.

The present study is concerned with the high pressure and high temperature behaviour of the electrical resistivity of Ti, Zr and Gd, primarily in the hcp phase ranges and at the transformation boundaries. Presented here are the data obtained for polycrystalline samples of Ti, Zr and Gd, and the applicability of these results in defining the pressure and temperature dependences of electrical resistivity, and in contributing to the mapping of their phase diagrams.

2. Experimental procedure

The purity of the polycrystalline specimens (AlfaAesar) was 99.99% for Ti, 99.5% for Zr and 99.9% for Gd. Except for machining, the high pressure experiments were carried out on the as-received samples. Zr and Gd sample bars and Ti wire were stored under vacuum to avoid oxidation. All samples were machined just before assembling the components of the high pressure cell and the start of the experimental run. The cylindrical sample geometry of 1 mm diameter $\times$6 mm length was kept constant for all experimental runs. The experiments were performed in a 1000 ton cubic anvil press, using 1 inch edge length pyrophyllite pressure cells, previously calibrated for pressure [45, 46].

The first set of high pressure resistivity measurements was performed at room temperature. Each specimen was placed in a sintered hexagonal boron nitride (hBN) cup. The sample was in contact with two double platinum electrodes, oriented at 90° to each other. The outside ends of the two double electrodes (four wires) were in direct contact with the four lateral tungsten carbide anvils of the press.

High pressure and high temperature resistivity measurements were carried out using a four wire configuration and a Pt/Pt–10% Rh thermocouple. Corrections for the pressure effect on the thermocouple were applied [47]. Heating of the sample was produced by the Joule effect using a large d.c. current sent through a cylindrical niobium (Nb) foil furnace, having the opposite top and bottom anvils of the press as electrodes. The sample in the hBN cup and the electrodes were placed in the centre of the cell, as shown in figure 2. Thermal insulation was provided by a cylindrical sleeve made of zirconia around the sample area.

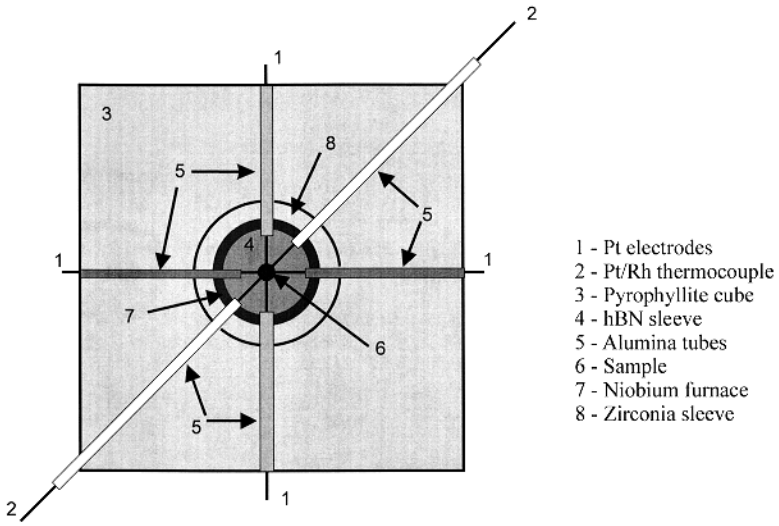

Figure 2. A cross-sectional view of the central plane of the high pressure cell used for continuous resistivity measurements at elevated temperature. The electrodes and the thermocouple are positioned on three different layers: one electrode and the thermocouple below the sample, a second electrode above the sample.

Two different configurations were employed in the design of the cell. One configuration was for continuous resistivity $\rho(P_{const}, T)$ measurements and another for discrete resistivity measurements in the isothermal–isobaric regime. Continuous data recording required the simultaneous use of the four Pt electrodes, with the temperature being measured and controlled by a through-gasket Pt/Pt–10% Rh thermocouple placed at 2–3 mm beneath the sample and lower electrode. All six wires (four electrodes and two thermocouple wires) were covered by alumina tubing to protect them from mechanical and electrical contact with the Nb foil heater. Outside the cell, the thermocouple wires were protected with Teflon tubing against electrical contact with the anvils. This configuration allowed for resistivity measurements while temperature was varied. The advantage of the continuous technique was that even the smallest variations in resistivity were recorded and P–T phase transformations were observed with high accuracy, as the system collected data at a sampling rate of 2 to 3 readings s^{-1}. The disadvantage was the damage of the alumina and Teflon insulation covering the thermocouple wires in the gasket regions, which resulted in electrical contact shorting between thermocouple and anvils. At pressures above 30 kbar, the through-gasket thermocouple wires started failing, unable to support the extensive shearing and compression in the gasket region combined with the stress produced by the outward flow of the pyrophyllite on temperature increase.

Measurements of resistivity for the Ti and Zr specimens were performed using the continuous recording approach, by increasing the pressure in steps of 2–4 kbar, and collecting data on both temperature increase and decrease at each pressure level. The heating and cooling rates were the same for both metals at all pressures.

The measurement of electrical resistivity of Gd at high pressures and temperature was performed using a discrete method of data recording. The configuration of the high pressure cell was changed, since the through-gasket thermocouple was eliminated—as shown in figure 3. One of the Pt electrodes was replaced with a Pt/Pt–10% Rh thermocouple, which performed the dual function of electrode and thermocouple. During temperature increase or decrease, when the furnace power supply required a temperature value as a feedback to control the

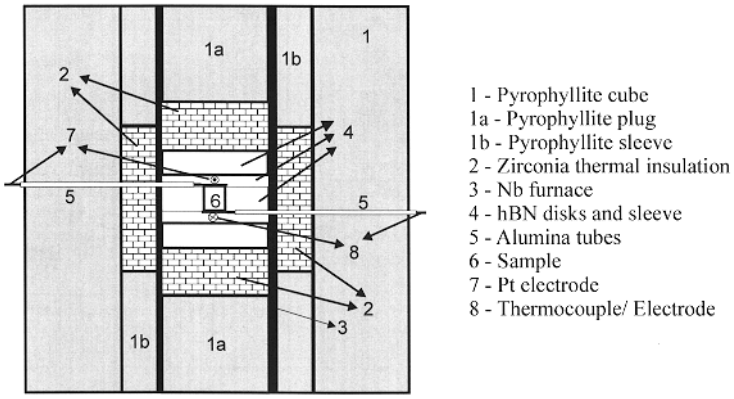

Figure 3. A cross-section of the high pressure cell used for discrete resistivity measurements at high temperature.

heating/cooling rate, the Pt/Pt–10% Rh wire acted as a thermocouple. But, at constant temperature, the Pt/Pt–10% Rh wire was used as a current and voltage electrode. The heating and cooling rate were maintained the same at each pressure level, and data were collected only after the system achieved thermal equilibrium at every temperature setting.

Except for pressure increase and decrease, the entire experiment was computer controlled, including the corrections for geometry and thermal expansion applied to the derived resistivity values.

3. Results and discussion

The measured resistance values were used to calculate the electrical resistivity. Geometry corrections corresponding to volume variation with pressure and temperature were applied to the entire data set, using the bulk modulus [48] and thermal expansion [49] values from table 1. The results for the pressure dependence of resistivity at room temperature are plotted in figures 4(a)–(c). All three metals exhibit similar behaviour, with resistivity decreasing with increasing pressure. Table 2 contains the values of the pressure coefficients of resistivity (PCRs) $\mathrm{d}\ln\rho/\mathrm{d}P$, calculated for both pressure increase and decrease, and compared with

Table 1. Bulk modulus K, $K' = (\mathrm{d}K/\mathrm{d}P)_T$ [48] and thermal expansion coefficients A_i [49].

	Ti	Zr	Gd	
K (kbar)	1094	1028	355	
$K' = (\mathrm{d}K/\mathrm{d}P)_T$	3.4	3.1	4.8	
A_0	−0.918	−0.111	−0.051	−0.373
A_1	5.072×10^{-4}	2.325×10^{-4}	6.381×10^{-4}	9.222×10^{-4}
A_2	6.50×10^{-7}	5.595×10^{-7}	5.446×10^{-7}	1.657×10^{-7}
A_3	-2.203×10^{-10}	1.768×10^{-10}	3.157×10^{-10}	1.347×10^{-9}
T interval for A_i (K)	$150 < T < 1156$	$293 < T < 1137$	$400 < T < 800$	$800 < T < 1200$

The linear thermal expansion is calculated using the above A_i coefficients and the following relations. Ti and Zr: $\Delta L/L_0 = A_0 + A_1T + A_2T^2 + A_3T^3$.
Gd, 400 K $< T <$ 800 K: $\Delta L/L_0 = A_0 + A_1(T-400) + A_2(T-400)^2 + A_3(T-400)^3$.
Gd, 800 K $< T <$ 1200 K: $\Delta L/L_0 = A_0 + A_1(T-800) + A_2(T-800)^2 + A_3(T-800)^3$.

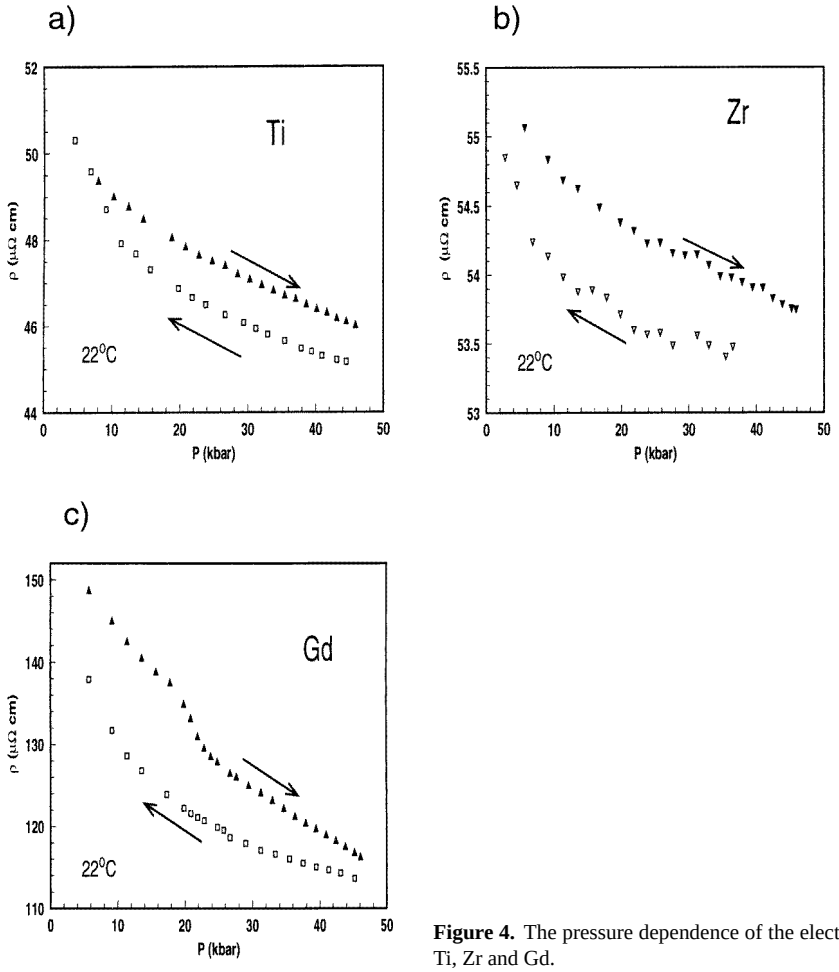

Figure 4. The pressure dependence of the electrical resistivity of Ti, Zr and Gd.

Bridgman's data [3, 4, 24]. All three metals show a delayed recovery of resistivity values on pressure decrease. For Ti and Zr above 10 kbar, the pressure increase and pressure decrease slopes seem to be almost parallel. At lower pressures, the curves approach very closely the initial resistivity values. This behaviour suggests hysteresis on pressure release, for the hcp phase only. At about 20–21 kbar and 22 °C, Gd undergoes a sudden decrease in resistivity, but returns to a less rapid decrease with pressure, as shown in figure 4(c). This variation is probably caused by a change from the ferromagnetic into the paramagnetic state associated with the hcp → Sm type structural phase transformation [25].

Isobaric runs were performed for the P–T range corresponding mainly to the hcp phase of the three metals and the transformation into neighbouring structures. Figures 5(a)–(c) show the variation of resistivity on heating at various pressures and the insets show typical heat/cool data sets. Each continuous line (Ti and Zr—figure 5(a) and (b)) or dotted line with symbols (Gd—figure 5(c)) represents a single isobaric run recorded on temperature increase only. The general trend for all three elements is an increase in the electrical resistivity with temperature and a decrease in the electrical resistivity with pressure. These results are typical of the metallic resistivity of a transition metal [50]. At high temperature, the electrical resistance of transition metals is mainly due to scattering processes in which the electron makes an s band to d band

Table 2. Pressure coefficients of electrical resistivity of Ti, Zr and Gd at room temperature.

	Ti	Zr	Gd
P_{max} (kbar)	46	47	46
$\mathrm{d}\ln\rho/\mathrm{d}P(\mathrm{kbar}^{-1})$ on $P_{increase}$	-1.54×10^{-3}	-5.97×10^{-4}	-6.03×10^{-3}
$\mathrm{d}\ln\rho/\mathrm{d}P(\mathrm{kbar}^{-1})$ on $P_{decrease}$	-1.51×10^{-3}	-5.66×10^{-4}	-4.17×10^{-3}
$\mathrm{d}\ln\rho/\mathrm{d}P(\mathrm{kbar}^{-1})$ Bridgman[a]	-1.48×10^{-3}	-7.7×10^{-4}	-5.7×10^{-3}
P interval (kbar)	20–46	5–36	5–46

[a]Bridgman's values were obtained from [55].

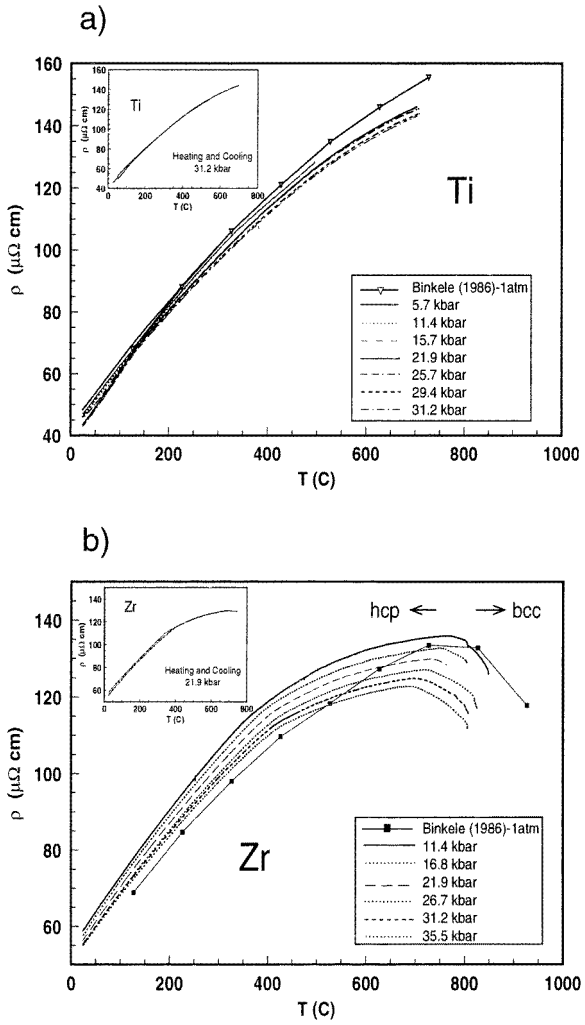

Figure 5. Electrical resistivity against temperature on isobaric runs for (a) Ti, (b) Zr and (c) Gd. Inset plots are selected isobars showing typical data on temperature increase and decrease.

transition [51]. The transition probability from one state to another is proportional to the density of unoccupied states in the final state [51]. Hence, transitions in which an electron jumps from the s band to an unoccupied state in the d band are more probable than the ordinary scattering processes. Therefore, the electrical resistivity is proportional to the ratio between

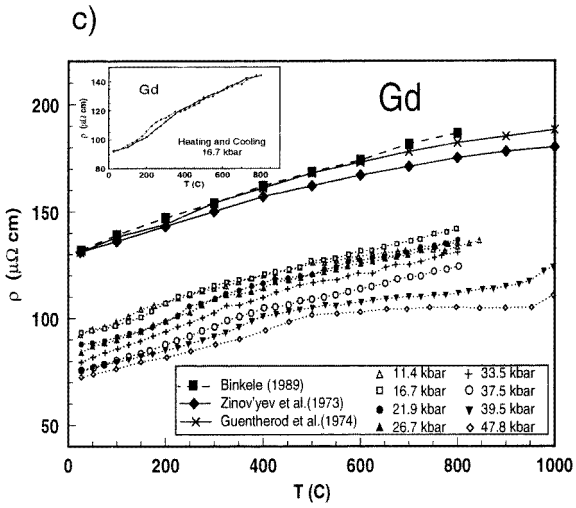

Figure 5. (Continued)

the cubed root of the number of empty states in the d band and the number of electrons in the s band. The outer electron configurations of the three metals in this study are the following: Ti, $3d^2 4s^2$; Zr, $4d^2 5s^2$; Gd, $4f^7 5d^1 6s^2$. The incomplete d and f bands give rise to a much larger scattering probability and hence a shorter mean free path. The density of unoccupied states in the d and f bands of Ti, Zr and Gd decreases slowly with the energy produced by heating of the sample. This could explain the downward concave shape of the $\rho(T)$ curves in figures 5(a)–(c) at high temperatures, especially in the case of Ti and Zr. At temperatures higher than the Debye temperature, the electronic resistance of metals is directly proportional to the mean square amplitude of the atomic vibrations [51]. Pressure has the effect of reducing the interatomic spacing of a metal, therefore lowering the amplitude of vibration, and hence the resistivity of the sample.

In their study of electrical resistivity of Gd, Jacobsson and Sundqvist [52] made the assumption that the total electrical resistivity is given by $\rho = \rho_0 + \rho_{ep} + \rho_m$, where ρ_0 is the residual resistivity at 0 K, ρ_{ep} is due to electron–phonon scattering and ρ_m is the component accounting for the electron–magnon scattering. Above room temperature, the values of ρ_0 and ρ_m are negligible by comparison with the phonon scattering effect. The value obtained for ρ_0 is 2.9 $\mu\Omega$ cm (only 2.2% of the 1 atm, 22 °C value) and is not temperature dependent. Therefore, the pressure and temperature effects on the phonon scattering of Gd are partly responsible for the behaviour of the resistivity in regions of stable polymorphism. A temperature increase produces an increase in the number of phonons and this causes an increase in the number of electron–phonon scattering events, resulting in an increase in the electrical resistivity. Pressure has the opposite effect, in that it reduces the interatomic spacing and the atomic vibrational amplitude, resulting in diminished scattering and resistivity. These antagonistic effects of temperature and pressure on $\rho_{Gd}(T, P)$ combine to give the observed behaviour.

Also shown in figures 5(a)–(c) are the $\rho(1\ \text{atm}, T)$ data obtained by Binkele [15, 31], Guentherodt *et al* [33] and Zinov'yev *et al* [53]. The low pressure curves of Ti maintain a shape that is in very good agreement with the curve obtained by Binkele [15]. Above 22 kbar, the resistivity–temperature curves change slope at relatively low temperatures (125–150 °C), due to the start of the temperature run from the dhcp phase, followed by the transformation into hcp. In figure 5(b), the electrical resistivity of Zr increases with temperature. The curves have a

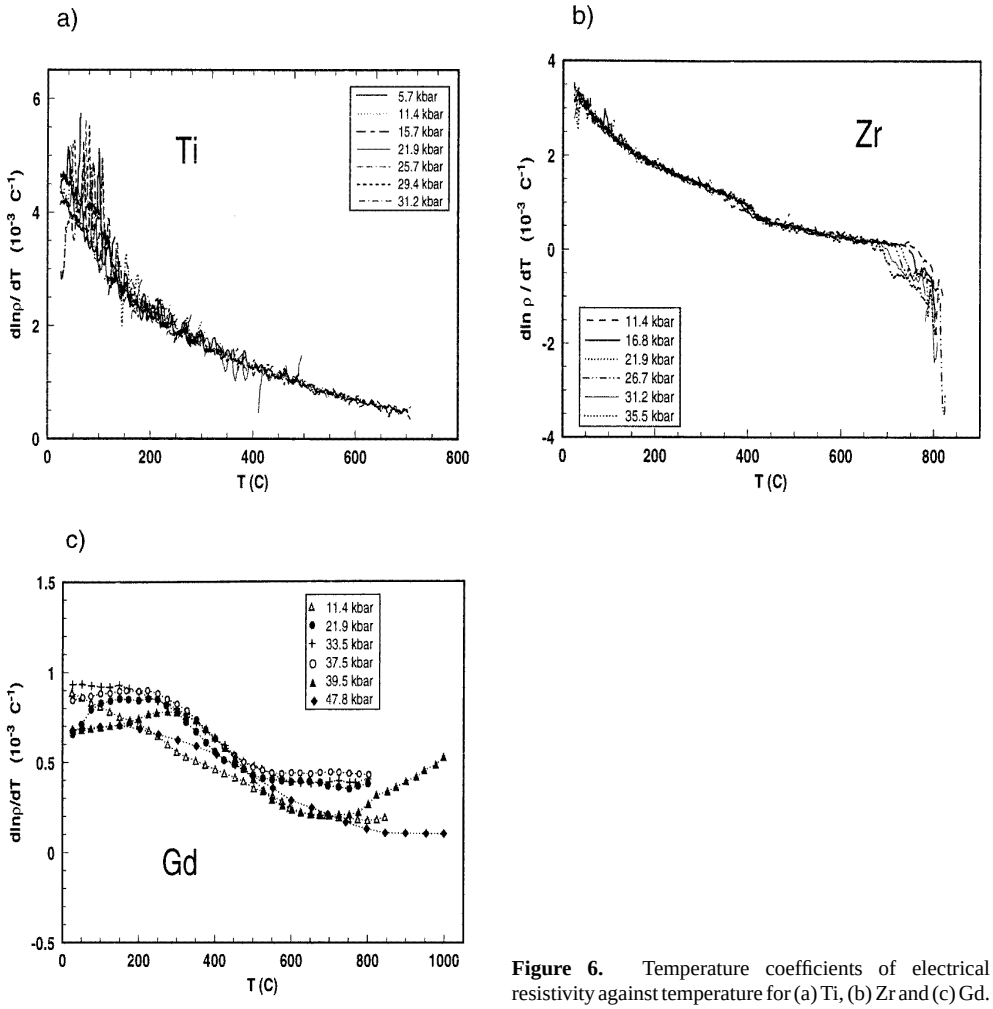

Figure 6. Temperature coefficients of electrical resistivity against temperature for (a) Ti, (b) Zr and (c) Gd.

shape very similar to Binkele's data at 1 atm, including the change in sign of the slope in the high temperature region signalling the hcp $\rightarrow$ bcc transformation. Our high pressure resistivity values for Zr are somewhat higher that expected, considering the 1 atm room temperature value. We speculate that this may be due to either an imperfect contact at the interface with the electrodes, a thin oxide layer resulting from the rapid oxidation of Zr or a small contribution from sample impurities. However, this difference in the resistivity value does not appear to affect the variation of electrical resistivity with pressure and temperature. In figure 5(c), the shape of the resistivity curves reflects the resistivity response of Gd as the sample 'travels' through different structural phase regions. Compared with Ti and Zr, there is a much larger gap between the 1 atm starting point and the high pressure runs. This behaviour may be explained by the fact that Gd is a much softer material, with a bulk modulus K, or inverse compressibility, that is approximately one third the value of K for Ti or Zr, as shown in table 1. The initial run, at 11.4 kbar, parallels the curves obtained by Binkele [31], Guentherodt *et al* [33] and Zinov'yev *et al* [53] at room pressure. Starting with the 16.7 kbar run, however, the data deviate from the linear trend, changing to smaller slope at about 225 °C. With increasing pressure, the change in slope can be observed at higher temperature values, suggesting the

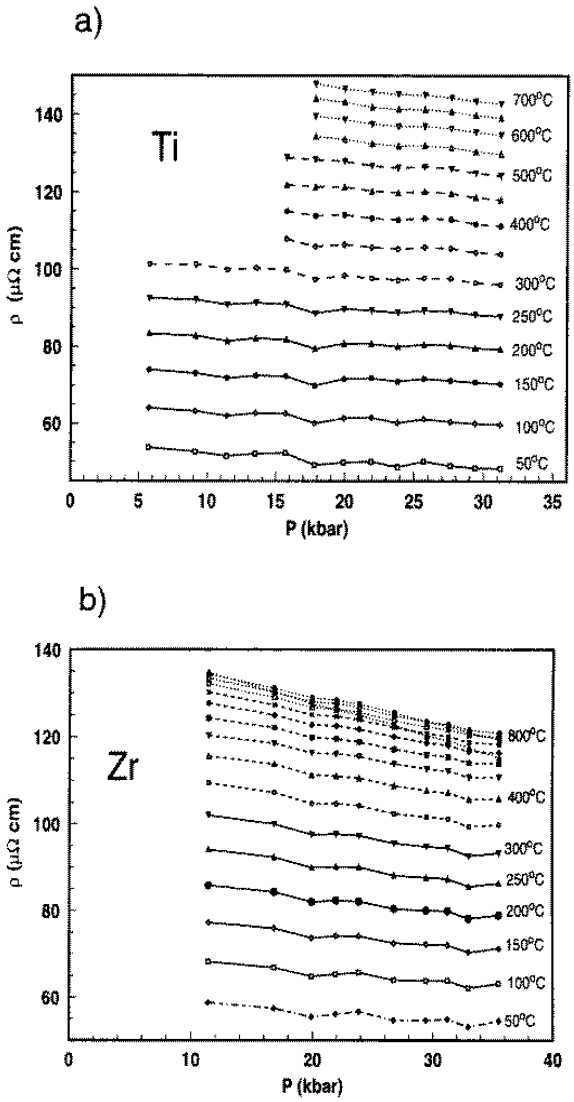

Figure 7. Isotherms of electrical resistivity against pressure for (a) Ti, (b) Zr and (c) Gd.

presence of a phase transformation with a positive sloping P–T boundary. The fact that the high temperature part of these curves resembles the slope of the 1 atm curves suggests that above 15–16 kbar the sample starts in the Sm-type phase and with temperature undergoes Sm type $\rightarrow$ hcp transformation. The 33.5 kbar isobar shows a second change in slope occurring at about 625 °C. This means that, while the temperature increase at 33.5 kbar is reflecting a Sm type $\rightarrow$ dhcp phase transition at 325 °C, the 625 °C resistivity change suggests a structural transformation from dhcp to hcp. Further increasing the pressure at 39.5 kbar, the shape of the curve and the changes in slopes indicate the Sm type $\rightarrow$ dhcp transformation at temperatures under 450 °C, while re-entry into the hcp phase (or the bcc phase) is achieved above 900 °C.

The temperature coefficient of the resistivity (TCR), $(\mathrm{d}\ln\rho/\mathrm{d}T)_p$, is plotted against temperature in figure 6. The TCR was obtained by differentiating the curves shown in

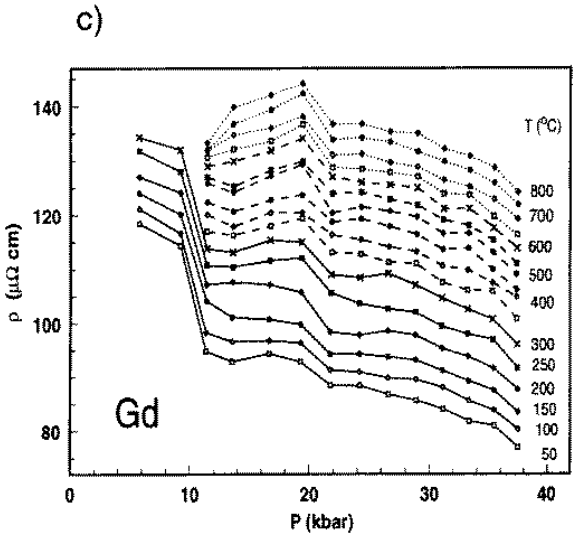

Figure 7. (Continued)

figures 5(a)–(c), using a 5 °C interval for the Ti and Zr continuous data, and a differentiation interval of approximately five sampling intervals for the discrete Gd data. The effect of temperature on the TCR of Ti, shown in figure 6(a), is effectively independent of pressure. The fluctuations in TCR values between 50 and 150 °C are a result of the small differentiation interval used for TCR derivation. In figure 6(b) the TCR of Zr in the hcp phase decreases with temperature and is also independent of pressure. The curve has a slightly smaller slope than that of Ti. The transformation into the high temperature bcc phase is reflected by the sudden drop in the TCR above 700 °C. The temperature of the drop in TCR decreases with increasing pressure, reflecting the negative P–T slope of the hcp $\rightarrow$ bcc transition. The anomalous change in slope observed for all pressures at $\sim$400 °C has not been observed in other studies. We speculate that the Zr sample is a 100% hcp phase only above 400 °C, while at lower temperatures, a small amount of dhcp is still present.

The TCR for polycrystalline Gd is shown in figure 6(c). The curves are much more scattered compared with Ti and Zr, but overall the fluctuations are on a smaller scale. The undulating trend of the data is mainly due to the presence of two and even three different phases at low temperatures and relatively low pressures. However, for the region of the curves corresponding to the hcp phase, the trend is a steady and almost linear decrease in temperature coefficient with increasing temperature.

The electrical resistivity data is presented against pressure along isotherms in figures 7(a)–(c). The interval between isotherms is 50 °C. The trend of resistivity decrease with pressure resembles the $\rho(22\,^{\circ}\mathrm{C}, P)$ curves shown in figures 4(a)–(c). In the highest pressure region of the three diagrams, the same steady decrease with pressure is observed. The slopes of the isotherms, PCR, were calculated for the entire P ranges shown in figure 7 and are plotted against temperature, for each metal, in figures 8(a)–(c). For Ti, the PCR increases with temperature below 150 °C, indicating the presence of a mixed hcp + dhcp phase. At higher temperature, in the hcp phase only, the pressure coefficient has an almost linear decrease with temperature. Above 600 °C the effect of temperature on the PCR disappears. Shown in figures 8(b) and (c) are the PCRs of Zr and Gd. The increase in the PCR of Zr between 375

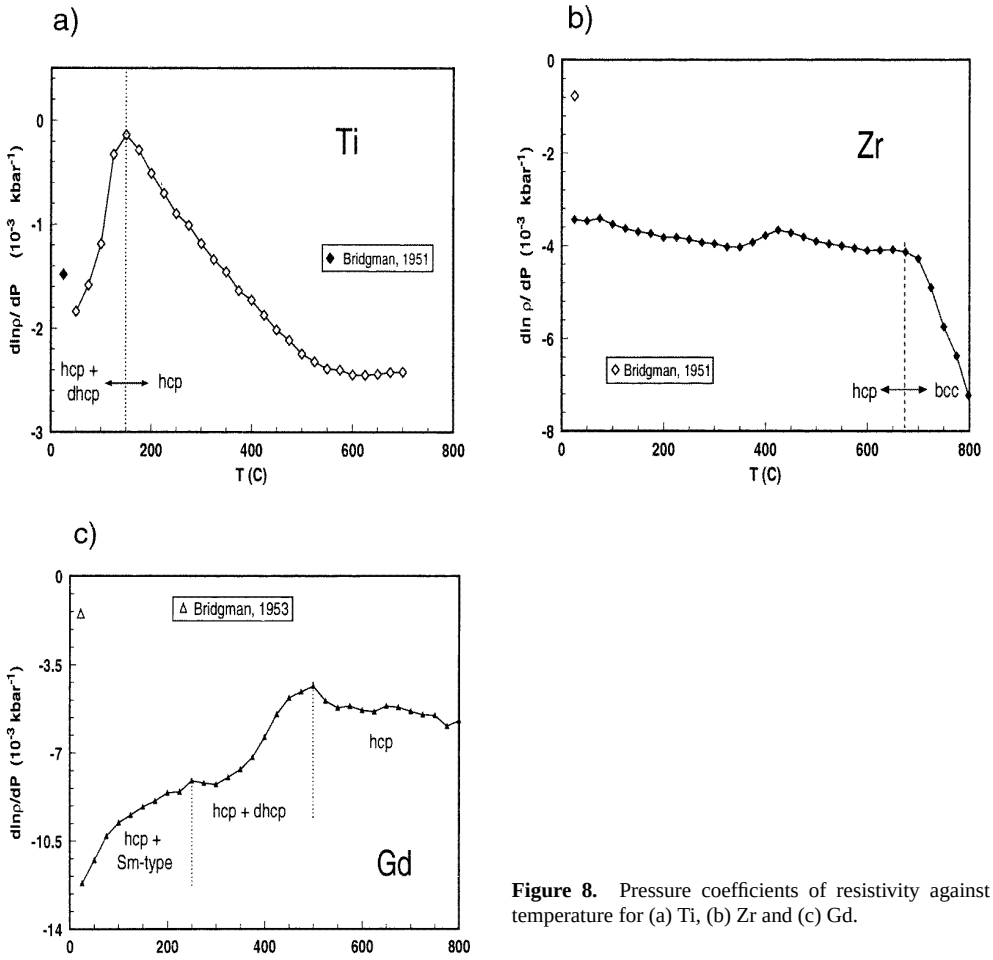

Figure 8. Pressure coefficients of resistivity against temperature for (a) Ti, (b) Zr and (c) Gd.

and 425 °C can be easily identified with the anomaly observed at the same temperature in the TCR plot, figure 6(b). However, the slope of the PCR against T up to 375 °C and from 425 to 725 °C is almost identical, indicating the presence of a dominant hcp phase. The sudden decrease in PCR above 725 °C is due to the high temperature hcp $\rightarrow$ bcc transformation. The PCR of Gd can be considered as being constructed from three different segments. At low temperatures, a mixed region of hcp and Sm-type phases is characterized by an increase in PCR with temperature, with downward concave shape. Above 250 °C, the phase 'budget' changes in favour of a combination of hcp and dhcp phases, with an upward concavity. At temperatures higher than 500 °C, the decrease in PCR with increasing temperature is very similar to the trends observed in the hcp phase regions of Ti and Zr, indicating the dominant presence of the hcp phase.

By combining the temperature dependence of resistivity and PCR, and the temperature dependence of resistivity and TCR, it is possible to identify boundaries between regions of the phase diagrams of Ti, Zr and Gd. Shown in figures 9(a)–(c) are the phase transformation boundaries studied for each metal. For Ti, the small changes in the slopes of the isobaric curves in figure 5(a) indicate that the hcp $\rightarrow$ dhcp transformation occurs at pressures above 20 kbar. The 5 °C kbar^{-1} slope of the boundary obtained in this study and shown in figure 9(a)

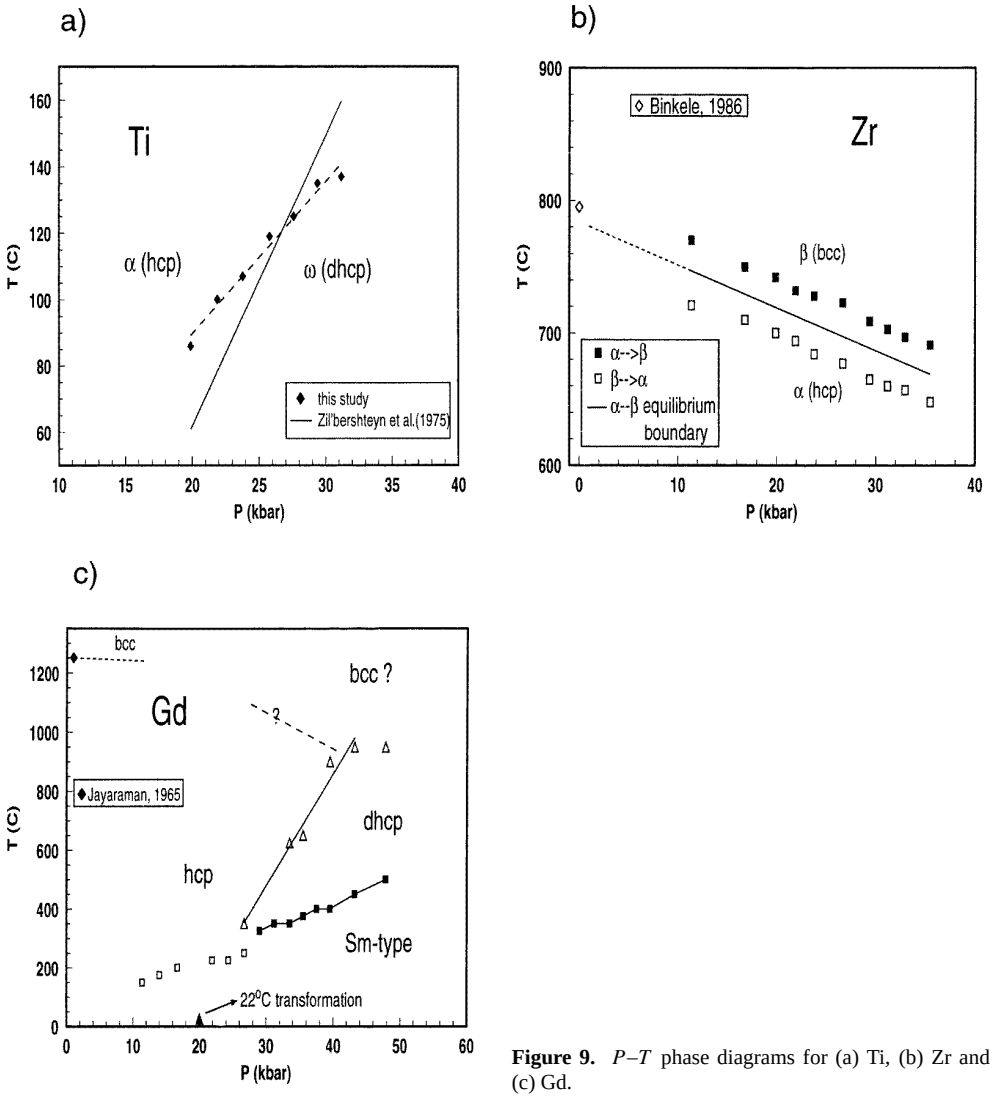

Figure 9. *P–T* phase diagrams for (a) Ti, (b) Zr and (c) Gd.

is smaller than the $9\,^{\circ}\mathrm{C\,kbar^{-1}}$ slope of the phase boundary (solid line) generally given in the literature [13, 39]. This result does encourage one to regard this curve as the start of the transformation, with the right hand side of the boundary being a mixture of the two phases.

The hcp $\rightarrow$ bcc high temperature phase transformation in Zr is shown in figure 9(b). The complete transformation of hcp into bcc (solid squares) and the complete reverse transformation from bcc into the hcp phase (open squares) bracket the equilibrium phase boundary. We chose the mid-point between the two complete transitions as the equilibrium phase boundary, as shown by the solid line. This extrapolation of the hcp $\rightarrow$ bcc equilibrium boundary determined in this study is in excellent agreement with Binkele's 1 atm value of the bcc transition [15].

For Gd, the phase boundaries constructed using the slope changes in figure 5(c) are more complex. Some of the isobaric runs contain two changes in curvature which are interpreted as a second phase boundary. Figure 9(c) was obtained by mapping out both sets of pressure–temperature coordinates, corresponding to the first and second changes in

slopes. The result can be interpreted as a transformation from hcp into the Sm-type phase observed at pressures as low as 12–15 kbar, which is much earlier than the 30 kbar pressure value predicted by the current phase diagram. This result confirms some of the more recent experimental values from the literature [40], which attest to the presence of Gd in an Sm-type phase at 15 kbar at 22 °C. It can be observed that at about 27–28 kbar there is a change in curvature of the constructed phase boundary (solid squares and continuous line curve in figure 9(c)). This change occurs simultaneously with the occurrence of a second set of data, reflecting the existence of a second phase boundary (open triangles and dotted line). One can attribute this second region at higher temperatures and higher pressures to the dhcp phase of Gd. We also speculate that the phase transformation occurring above 40 kbar and 950 °C is from dhcp into either hcp or bcc. The solid triangle placed at the bottom of the diagram corresponds to the well observed transition at 20 kbar in the room temperature run shown in figure 4(c). It was previously proposed that a variation in electrical resistivity between 21.5 and 26.7 kbar is associated with the change from a ferro- to paramagnetic state occurring simultaneously with the structural phase transformation from hcp into the Sm-type phase, due to the effect of changes in interatomic distance on the magnetic behaviour [52]. We consider our result at 20 kbar (solid triangle in figure 9(c)) to be in good agreement with these previous observations. We interpret the changes in electrical resistivity of Gd in the 11–26 kbar pressure interval (open squares in figure 9(c)) as being the result of a second order magnetic effect, and less likely a structural transformation. The curvature of $\rho(T, P)$ in figure 5(c) is similar to the one obtained by plotting the temperature dependence of the magnetic spin component of the electrical resistivity of Gd calculated for 1 atm [54].

4. Conclusions

New experimental data have been obtained for the pressure and temperature effects on electrical resistivity of pure Ti, Zr and Gd metals. The electrical resistivity of all three transition metals increases with temperature increase and decreases with pressure increase. The separate effects of both pressure and temperature were determined by calculating the pressure and temperature coefficients. The temperature coefficient–temperature diagrams of all three metals suggest that in the hcp phase the temperature effect on resistivity is independent of pressure. The pressure coefficients of resistivity decrease with increasing temperature in the hcp region. In addition, plots of these coefficients have brought additional information regarding the phase transitions from the hcp into the neighbouring phases. The resistivity changes corresponding to the hcp $\rightarrow$ dhcp transition of Ti and the hcp $\rightarrow$ bcc transformation of Zr are in good agreement with previous experimental data. New information has been obtained for the Gd phase transitions between 10 and 50 kbar and at temperatures up to 950 °C.

Acknowledgments

We thank R Tucker for technical help with the pressure cells and the referees for helpful comments. This work was supported by a Natural Sciences and Engineering Research Council of Canada grant to RAS.

References

[1] Liu L-G and Bassett W A 1986 *Elements, Oxides, and Silicates. High-Pressure Phases with Implications for the Earth's Interior* (New York: Oxford University Press)

[2] Tonkov E Yu 1992 *High Pressure Phase Transformations. A Handbook* (London: Gordon and Breach)

[3] Bridgman P W 1951 *Proc. Am. Acad. Arts Sci.* **79** 149
[4] Bridgman P W 1952 *Proc. Am. Acad. Arts Sci.* **81** 167
[5] Jamieson J C 1963 *Science* **140** 72
[6] Jayaraman A, Klement W and Kennedy G C 1963 *Phys. Rev.* **131** 644
[7] Kutsar A R, German V N and Nosova G I 1974 *Sov. Phys.–Dokl.* **18** 733
[8] Olinger B and Jamieson J C 1973 *High Temp.–High Pressure* **5** 123
[9] Sargent G A and Conrad H 1971 *Mater. Sci Eng.* **7** 220
[10] Usikov M P and Zil'bershteyn V A 1973 *Phys. Status Solidi* A **19** 53
[11] Vohra Y K 1978 *J. Nucl. Mater*. **75** 288
[12] Xia H, Parthasarathy G, Luo H, Vohra K Y and Ruoff A L 1990 *Phys. Rev.* B **42** 6736
[13] Zil'bershteyn V A, Nosova G I and Estrin E I 1973 *Fiz. Met. Metalloved.* **35** 584
[14] Andersson S 1959 *Acta. Chem. Scand.* **13** 415
[15] Binkele L 1986 *High Temp.–High Pressure* **18** 599
[16] Guillermet A F 1987 *High Temp.–High Pressure* **19** 119
[17] Timrot D L and Peletskii V E 1965 *Teplofiz. Vis. Temp.* **3** 223
[18] Wasilewski R J 1962 *Trans. Metall. Soc. AIME* **224** 5
[19] White G K and Woods S B 1959 *Proc. R. Soc.* A **251** 273
[20] Zinov'yev V E 1979 *Sov. Phys.–Solid State* **20** 1298
[21] Zhorov G A 1969 *Teplofiz Vis. Temp.* **8** 532
[22] Secco R A, Manghnani M H, Ming L C, Li X and Xu J A 1993 *High Pressure Research: Application to Earth and Planetary Sciences*, ed Y Syono and M H Manghnani (Tokyo: Terrapub/Washington, DC: AGU) p 477
[23] Vaidya S N and Kennedy G C 1972 *J. Phys. Chem. Solids* **33** 1377
[24] Bridgman P W 1953 *Proc. Am. Acad. Arts Sci.* **82** 83
[25] McWhan D B and Stevens A L 1965 *Phys. Rev.* **139** 682A
[26] Wakabayashi I, Kobayashi H, Nagasaki H and Minomura S 1968 *J. Phys. Soc. Japan* **25** 227
[27] Belov K P, Ergin Yu, Katsnel'son A A and Ped'ko V 1965 *Pis. Eksp. Teor. Fiz.* **1** 8
[28] Jayaraman A and Sherwood R C 1964 *Phys. Rev.* **134** A691
[29] Tonkov E Yu, Aptekar I L, Degtyareva V F and Krasavin Yu 1976 *Dokl. Akad. Nauk* **230** 85
[30] Spedding F H, Hanak J J and Daane A H 1961 *J. Less-Common Met.* **3** 110
[31] Binkele L 1989 *High Temp–High Pressure* **21** 131
[32] Birss R R and Dey S K 1961 *Proc. R. Soc.* A **263** 473
[33] Guentherodt H-J, Hauser E and Kunzi H U 1974 *Phys. Lett.* A **47** 189
[34] Nellis W J and Legvold S 1969 *J. Appl. Phys.* **40** 2267
[35] Gel'd P V and Zinov'yev V E 1976 *High Temp.–High Pressure* **8** 523
[36] Maezawa K, Mori K, Sato K, Saito Y and Wakabayashi S 1977 *J. Phys. Soc. Japan* **43** 1815
[37] Nellis W J and Legvold S 1969 *Phys. Rev.* **180** 581
[38] Nigh H E, Legvold S and Spedding F H 1963 *Phys. Rev.* **132** 1092
[39] Zil'bershteyn V A, Chistotina N P, Zharov A A, Grishina N S and Estrin E I 1975 *Fiz. Met. Metallov.* **39** 445
[40] Stager R A and Drickamer H G 1964 *Phys. Rev.* **133** A830
[41] Akella J, Smith G S and Jephcoat A P 1988 *J. Phys. Chem. Solids* **49** 573
[42] Fujii H, Tani H, Okamoto T and Tatsumoto E 1972 *J. Phys. Soc. Japan* **33** 855
[43] Stephens D R 1965 *J. Phys. Chem. Solids* **26** 943
[44] Stromberg H D and Stephens D R 1964 *J. Phys. Chem. Solids* **25** 1015
[45] Secco R A 1994 *High Pressure Science and Technology*, vol 2, ed S C Schmidt, J W Shaner, G A Samara and M Ross (New York: AIP) p 1593
[46] Secco R A 1995 *Can. J. Phys.* **73** 287
[47] Bundy F P 1961 *J. Appl. Phys.* **32** 403
[48] Knittle E 1995 *Mineral Physics and Crystallography. A Handbook of Physical Constants (AGU Reference Shelf 2)* ed T J Ahrens (Washington, DC: American Geophysical Union) p 98
[49] Touloukian Y S, Kirby R K, Taylor R E and Desai P D 1970 *Metallic Elements and Alloys (Thermophysical Properties of Matter 12)* IFI/Plenum, New York
[50] Secco R A and Schloessin H H 1989 *J. Geophys. Res.* **94** 5887
[51] Mott N F and Jones H 1958 *The Theory of the Properties of Metals and Alloys*, Dover, New York
[52] Jacobsson P and Sundqvist B 1989 *Phys. Rev.* B **40** 9541
[53] Zinov'yev V Ye, Gel'd L P, Chuprikov G Ye and Yepifanova K I 1973 *Sov. Phys.–Solid State* **14** 2372
[54] De Gennes P G and Friedel J 1958 *J. Phys. Chem. Solids* **4** 71
[55] *Landolt–Börnstein New Series* 1985 vol 15b (Berlin: Springer) p 13
[56] Jayaraman A 1965 *Phys. Rev.* **139** A690